

# Frontiers in atomistic simulations of high entropy alloys

Cite as: J. Appl. Phys. **128**, 150901 (2020); <https://doi.org/10.1063/5.0025310>

Submitted: 14 August 2020 . Accepted: 01 October 2020 . Published Online: 20 October 2020

 Alberto Ferrari,  Biswanath Dutta,  Konstantin Gubaev,  Yuji Ikeda,  Prashanth Srinivasan,  Blazej Grabowski, and  Fritz Körmann



View Online



Export Citation



CrossMark

## ARTICLES YOU MAY BE INTERESTED IN

[Electronic structure spectroscopy of organic semiconductors by energy resolved-electrochemical impedance spectroscopy \(ER-EIS\)](#)

Journal of Applied Physics **128**, 150902 (2020); <https://doi.org/10.1063/5.0022289>

[Computer aided design of stable and efficient OLEDs](#)

Journal of Applied Physics **128**, 160901 (2020); <https://doi.org/10.1063/5.0022870>

[Beyond Graphene: Low-Symmetry and Anisotropic 2D Materials](#)

Journal of Applied Physics **128**, 140401 (2020); <https://doi.org/10.1063/5.0030751>



Learn how to perform the readout of up to 64 qubits in parallel

With the next generation of quantum analyzers on November 17th

Register now



# Frontiers in atomistic simulations of high entropy alloys

Cite as: J. Appl. Phys. 128, 150901 (2020); doi: 10.1063/5.0025310

Submitted: 14 August 2020 · Accepted: 1 October 2020 ·

Published Online: 20 October 2020



View Online



Export Citation



CrossMark

Alberto Ferrari,<sup>1,a)</sup>  Biswanath Dutta,<sup>1</sup>  Konstantin Gubaev,<sup>1</sup>  Yuji Ikeda,<sup>2</sup>  Prashanth Srinivasan,<sup>1</sup>   
Blazej Grabowski,<sup>2</sup>  and Fritz Körmann<sup>1,3</sup> 

## AFFILIATIONS

<sup>1</sup>Materials Science and Engineering, Delft University of Technology, 2628CD Delft, The Netherlands

<sup>2</sup>Institute for Materials Science, University of Stuttgart, 70569 Stuttgart, Germany

<sup>3</sup>Max-Planck-Institut für Eisenforschung GmbH, 40237 Düsseldorf, Germany

<sup>a)</sup>Author to whom correspondence should be addressed: A.Ferrari-1@tudelft.nl

## ABSTRACT

The field of atomistic simulations of multicomponent materials and high entropy alloys is progressing rapidly, with challenging problems stimulating new creative solutions. In this Perspective, we present three topics that emerged very recently and that we anticipate will determine the future direction of research of high entropy alloys: the usage of machine-learning potentials for very accurate thermodynamics, the exploration of short-range order and its impact on macroscopic properties, and the more extensive exploitation of interstitial alloying and high entropy alloy surfaces for new technological applications. For each of these topics, we briefly summarize the key achievements, point out the aspects that still need to be addressed, and discuss possible future improvements and promising directions.

Published under license by AIP Publishing. <https://doi.org/10.1063/5.0025310>

## I. INTRODUCTION

High entropy alloys (HEAs),<sup>1-3</sup> more broadly referred to as compositionally complex alloys, are metallic mixtures of several elements in non-dilute concentrations. HEAs are typically nearly-equiatomic alloys of four, five, or more components with similar atomic radii and low mixing enthalpies and, despite the chemical complexity, are characterized by simple structures (fcc, bcc, or hcp solid solutions, even at room temperature) with often remarkably better mechanical properties than the elemental components.<sup>4-11</sup> Original works on HEAs suggested the large configurational entropy as the driving force behind the formation of simple solid solutions, hence their name, but it was proved later that these solutions are, in most cases, only metastable.<sup>12</sup>

Atomistic simulations of HEAs, based on first principles calculations or interatomic potentials, are complicated by a large number of constituents that entail a combinatorially high computational (and in some cases human) effort. Modeling HEAs from first principles is challenging because of the difficulty to sample chemical (and possibly magnetic) disorder: typical setups employ either finite supercells that may introduce spurious ordering effects due to periodic boundary conditions or mean-field approximations that

neglect local effects such as atomic relaxations. Modeling HEAs with interatomic potentials, on the other hand, requires the parameterization of the multi-body interactions among several atomic species, which in turn necessitates extensive training databases, flexible potentials, and robust, efficient, and, preferably, fully automated fitting strategies, whose implementation is usually far from straightforward.

Early atomistic simulations of HEAs focused on phase stability, magnetic arrangement (especially in alloys of the Cr-Mn-Fe-Co-Ni family), short-range order, elasticity, local lattice distortions, and stacking fault energies. Comprehensive reviews on atomistic simulations of HEAs are provided, for instance, in Refs. 13 and 14. Rather than offering a broad overview of what has been done in the past, in this Perspective we selected three aspects of atomistic simulations of HEAs that very recently experienced the most substantial advancements and that we anticipate will be key topics in the immediate future of HEAs: (i) the accuracy boost in thermodynamic calculations arising from the usage of machine-learning potentials (Sec. II), (ii) the more mature understanding of the consequences of short range order on macroscopic quantities (Sec. III), and (iii) the characterization and utilization of defects: interstitials and surfaces (Sec. IV).

These three topics demonstrate how quickly the atomistic modeling of HEAs evolved from more general simulations toward very elaborate applications, which are difficult to explore from experiments alone, for example, chemical short-range order. They also reveal how severe approximations in the early simulations can nowadays be overcome. For instance, phase diagram calculations do not need to involve harmonic or quasi-harmonic approximations, solid solutions are not treated as fully disordered anymore, varying the compositional phase space may also include interstitial defects, and not only bulk but also surface calculations can be addressed.

Since in the present Perspective we focus on atomistic simulation of metallic alloys, we intentionally neglect other important aspects of modeling HEAs that flourished in the recent years. One example is the data-driven design of HEAs: as the availability of data on HEAs is rapidly growing, a variety of descriptors and machine-learning algorithms are being used to guide the exploration of the multidimensional composition space of HEAs, often leading to the discovery of new materials.<sup>15–21</sup> There are also interesting materials classes related to HEAs which we on purpose do not discuss. To give one example, high entropy ceramics were recently explored for the most disparate applications, as detailed in Ref. 22.

## II. ACCURATE THERMODYNAMICS: THE MACHINE LEARNING REVOLUTION

### A. Machine-learning potentials for HEAs and active learning

Given the large number of adjustable parameters in the functional form, machine-learning potentials are extremely flexible and thus outperform classical potentials or force fields in terms of accuracy, *albeit* often at the expense of transferability and interpretability.

The idea of exploiting multiparameter models to represent the interatomic interaction is not new<sup>23,24</sup> and the utilization of machine-learning potentials was, at least at the beginning, gradual and limited to simple systems. The application to HEAs was later enabled by two factors: (1) the emergence of a great variety of machine-learning approaches based on different mathematical formalisms,<sup>23–31</sup> some of which turned out to work better than others for multicomponent alloy systems; (2) the advancement in the computational infrastructure to produce and store large amounts of computational data also for more complex alloys, facilitated by the organization of data in databases and repositories<sup>32–35</sup> that also promoted knowledge transfer and data mining.

The major challenge in the parametrization of machine-learning potentials for HEAs remains the availability of data: for simpler systems, reference data can be computed manually or semi-automatically, but the chemical disorder in HEAs complicates substantially this task because of the combinatorially high number of possible configurations (*curse of dimensionality* in the machine-learning jargon). An inevitable incompleteness of the training set in this case may lead to severe overfitting and large extrapolation errors. Moreover, even if a machine-learning potential is somehow obtained, it is not always clear exactly what data are needed to improve the model.

A possible solution to the incompleteness of the training set is active learning (AL): within AL, new training instances are suggested automatically in order to maximize the accuracy of the machine-learning potential and to avoid extrapolation into unexplored territory, the latter being a key challenge in the exploration of the complex structure-energy landscape of HEAs. The advantage is that the calculation of the suggested structures can be performed on-the-fly during a simulation, meaning that only the structures that are highly relevant for the simulation enter the (time-dependent) fitting database. The disadvantage is that the obtained machine-learning potentials are often hardly transferable to other simulations unless fitting or active learning are performed again.

An intuitive approach for estimating the uncertainty of a prediction of a machine-learning potential is to train an ensemble of models, incorporating some randomness in the fitting, and define the points of maximum uncertainty as those at which different models disagree the most.<sup>36,37</sup> These points will then be the optimal candidates to extend the training database. However, this way of estimating the uncertainty may be biased by the fact that the models, being trained on the same data, are never fully statistically independent from each other.

Another method,<sup>38–40</sup> termed Bayesian AL, is used in combination with Gaussian kernel-based machine-learning models, such as the Gaussian approximation potentials.<sup>25</sup> The fitting coefficients entering these models are determined from a set of observations at points  $\{X_j\}$  in the space of descriptors. The prediction for any other point  $x$  is then made based on how  $x$  overlaps with the known parts of the descriptor space  $\{X_j\}$ : the less overlap is observed, the more uncertainty is associated with the prediction. This overlap is usually quantified in terms of the Smooth Overlap of Atomic Positions descriptors.<sup>41</sup> If the uncertainty of the prediction at  $x$  is larger than a defined threshold, the configuration corresponding to  $x$  is added to the fitting database and the model is retrained.

Alternatively, a geometric non-probabilistic AL approach<sup>42</sup> was proposed for moment tensor potentials (MTPs).<sup>29</sup> For these potentials, the fitting equations take the form

$$A(\mathbf{x})\boldsymbol{\theta} = \mathbf{r}(\mathbf{x}), \quad (1)$$

where

$$A = \begin{pmatrix} b_1(\mathbf{x}^{(1)}) & & b_m(\mathbf{x}^{(1)}) \\ \vdots & \ddots & \vdots \\ b_1(\mathbf{x}^{(n)}) & & b_m(\mathbf{x}^{(n)}) \end{pmatrix} \quad (2)$$

is the matrix of the basis functions  $b_k$ ,  $\boldsymbol{\theta} = (\theta_1, \dots, \theta_m)$  is the vector of fitting coefficients, and  $\mathbf{r} = (E(\mathbf{x}^{(1)}), \dots, E(\mathbf{x}^{(n)}))$  contains the reference energies.

The geometric AL approach for MTPs assumes that  $\mathbf{r}$  contains some noise and proposes to choose  $A$  so that the noise in the fitting coefficients  $\boldsymbol{\theta}$  is minimized. It can be shown that such an approach leads to maximizing the determinant of  $A$ , i.e., the volume of the training domain in the space of  $b_k$  (see Fig. 1).

At the present stage, AL was employed for molecules, simple metals, and intermetallic compounds to fine-tune or optimize the training database. But the formalism can be easily extended to HEAs, for simulations within completely unexplored regions of

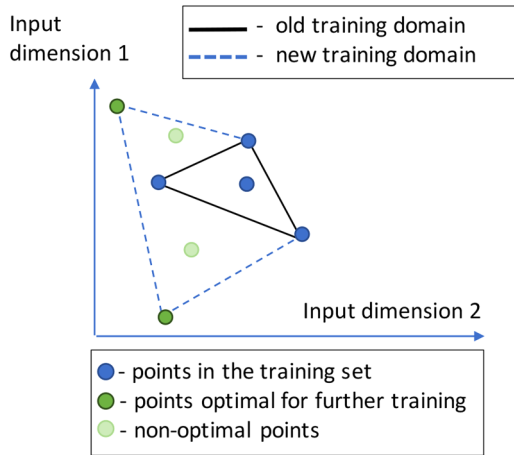


**FIG. 1.** Pictorial representation of the geometric criterion employed for AL with MTPs. The optimal training set is the one maximizing the volume of the domain, ensuring interpolation for as many points as possible.

configurational space, where the problem of incomplete training databases is so severe that one needs to rely on data-driven approaches rather than heuristics. In parallel, the application of machine learning potentials to multicomponent alloys is becoming more and more common, as the examples provided in Subsection II B attest, highlighting the huge potential of these techniques for further exploration of HEAs.

## B. Application to thermodynamics

A field that vastly benefited from the usage of machine-learning potentials is the calculation of thermodynamic properties, such as phase stabilities and phase diagrams, and other temperature-dependent quantities. The main reason for the good performance of interatomic potentials, in particular, of machine-learning potentials, for predicting high temperature thermodynamics is the localization of the interactions in the system at finite temperatures:<sup>43,44</sup>  $T = 0$  K long-ranged quantum mechanical interactions often disappear when atomic vibrations are introduced and crystal symmetry is broken, hence the free energies at high temperature can be calculated from a well-defined and local part of the phase space—a task that is ideally suited for potentials characterized by a finite distance cutoff.

The superior accuracy of machine-learning potentials for HEAs was demonstrated in a recent work<sup>45</sup> where an MTP was fitted to calculate the free energy of the bcc refractory NbMoTaVW HEA at 3000 K up to DFT accuracy. Numerically exact vibrational free energies were obtained by a two-stage thermodynamic integration using Langevin dynamics (TU-TILD) technique,<sup>46</sup>

$$F = F^{\text{ref}} + \int_0^1 d\lambda_1 \langle E^{\text{MTP}} - E^{\text{ref}} \rangle_{\lambda_1} + \int_0^1 d\lambda_2 \langle E^{\text{DFT}} - E^{\text{MTP}} \rangle_{\lambda_2}, \quad (3)$$

where the MTP with energies  $E^{\text{MTP}}$  acts intermediately between DFT and an analytical reference potential, such as the quasiharmonic approximation, with energy  $E^{\text{ref}}$  and free energy  $F^{\text{ref}}$ , and  $\langle \dots \rangle_{\lambda}$  signifies a thermodynamic ensemble average on the mixed potential  $E^{\lambda} = \lambda E^{\text{DFT}} + (1 - \lambda) E^{\text{MTP}}$ . The TU-TILD approach explored in that work was successful and rapid owing to the ability to fit very accurate MTPs that resemble DFT data, thereby making the more expensive second stage of the TU-TILD much faster. This method helps to go beyond the quasi-harmonic approximation by taking into account the high-temperature anharmonic effects that, especially in refractory elements/alloys, are as significant as the electronic contributions at high temperature.

The method has also been applied to various bcc refractory alloys ranging from two- to five-component alloys. Figure 2(a) shows the accuracy of the MTPs in the calculation of the free energy for four such alloys. For the sake of comparison, the free energy difference obtained with an embedded atom method (EAM) potential<sup>47,48</sup> is also displayed for the five-component system. Besides, Figs. 2(b) and 2(c) report the force correlations between DFT and EAM, and DFT and MTP, respectively. The actual fitting and construction of the MTPs has taken less computational time (by an order of magnitude) as compared to that for the EAM and the predicted values of

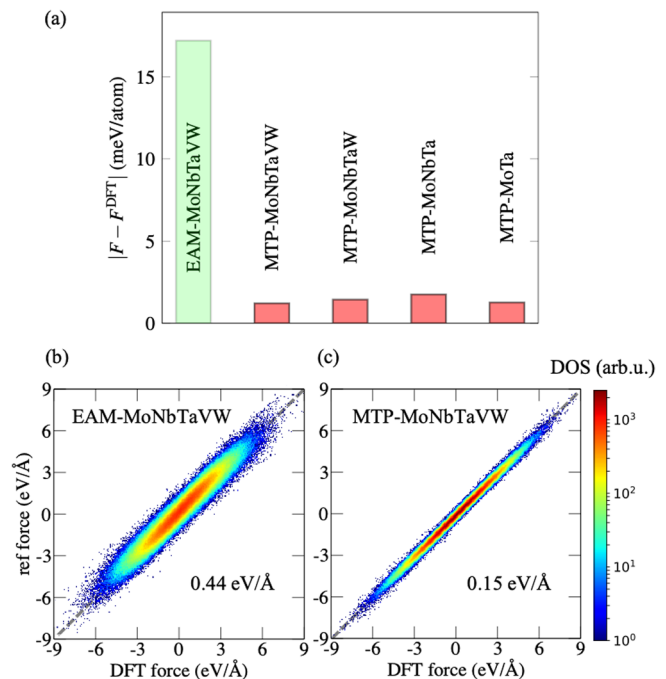


**FIG. 2.** (a) Free energy differences for various bcc refractory HEAs from atomic vibrations predicted by MTPs vs EAM at 3000 K revealing MTPs predictive power. Correlation between DFT forces vs forces predicted by the (b) EAM and (c) MTP for the MoNbTaVW alloy at 3000 K. The color represents local density. The root mean square error of the distributions is provided in the inset. Reproduced from Grabowski *et al.*, NPJ Comput. Mater. 5, 80 (2019). Copyright 2019 Author(s), licensed under a Creative Commons Attribution (CC BY) license.

the free energy are within 2 meV/atom of DFT, an order of magnitude more accurate than EAM. The root mean square error in the forces predicted by the MTP is one-third of that predicted by the EAM. These promising results instill confidence in systematically extending the fitting of machine-learning potentials to arbitrary compositions and crystal structures.

Other examples in the recent literature confirm the success of machine-learning potentials for the analysis of the high-temperature properties of HEAs: low rank potentials<sup>49</sup> were used to investigate the phase diagrams of bcc MoNbTaW and fcc CrFeCoNi with Monte Carlo simulations<sup>50,51</sup> and the formation of new structures was observed in both cases; a neural network potential was exploited to study a refractory high entropy melt;<sup>52</sup> and local lattice distortions and elastic constants were calculated at finite temperature with another MTP for the fcc medium entropy alloy FeCoNi.<sup>53</sup>

With the current methodology and the predictive capabilities of machine-learning potentials, total free energies can be efficiently calculated at different temperatures and volumes, including accurate anharmonic contributions. From this, free energy surfaces can be obtained for novel HEAs from which material properties like the bulk modulus, heat capacities, and thermal expansions can be accurately computed. With a combination of molecular dynamics and Monte Carlo techniques, phase diagrams could also be evaluated, simplifying the exploration of the complex compositional space of HEAs and thus serving as an optimization tool for the design of new alloys.

### III. SHORT RANGE ORDER IMPACTS THE PROPERTIES OF HEAs

Early atomistic simulations of HEAs usually assumed that these metals form random solid solutions [Fig. 3(a)] and consistently modeled perfectly disordered configurations either with mean-field approaches, such as the coherent potential approximation,<sup>54,55</sup> or with particular supercells that mimic the multi-body correlations of random configurations, such as special quasirandom structures or related concepts.<sup>56–59</sup> This is a realistic approximation at high temperature, where the configurational entropy dominates all the other contributions to the free energy; at lower temperature, instead, the distribution of the atoms deviates from random as multiplets of elements arrange in specific, energetically more favored configurations that lower the degree of disorder, giving rise to spatial correlations. If these spatial correlations are long-ranged, they could lead to clustering and phase separation [Fig. 3(c)], whereas if they are short-ranged [Fig. 3(b)], they produce short range order (SRO).

SRO is usually quantified in terms of pairwise correlations between species  $i$  and  $j$  with the Warren–Cowley parameters<sup>60,61</sup>

$$\alpha_{ij}^m = 1 - \frac{P_{ij}^m}{c_i c_j}, \quad (4)$$

with  $P_{ij}^m$  being the probability to find the pair  $i$ – $j$  in the  $m$ th pair cluster (shell) and  $c_i$  and  $c_j$  being the concentrations of  $i$  and  $j$ . As an example, we show in Fig. 4 the temperature dependence of the Warren–Cowley parameters for the first shell of four different pairs

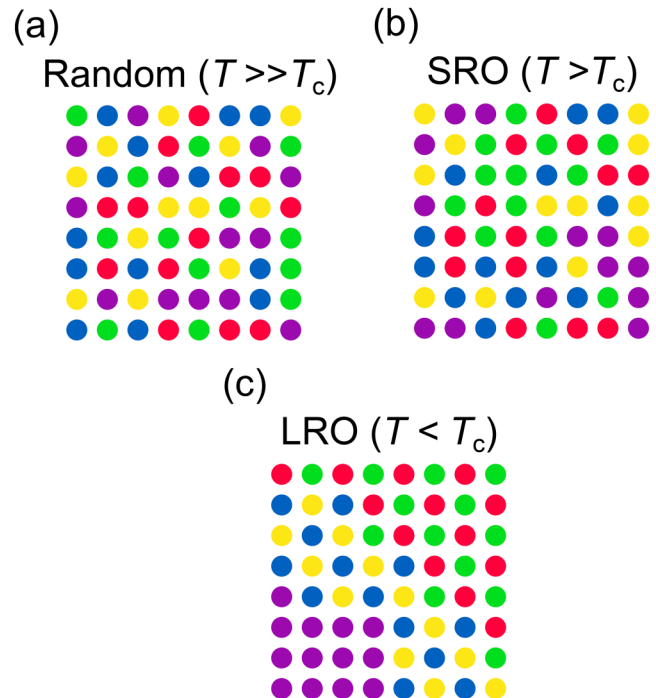


**FIG. 3.** (a) Random configuration of the elements in a quinary HEA at a temperature much higher than the critical ordering temperature ( $T_c$ ). (b) Short range order at an intermediate temperature: multiplets of neighboring atoms (e.g., pairs of red–green, red–blue, and purple–purple) are favored over other combinations. (c) Long range order induces separation of three phases at a temperature lower than  $T_c$ .

in the quaternary MoNbTaW HEA.<sup>50</sup> For this alloy, if atomic relaxation is not taken into account for simplicity, the two phases B2 (Mo,Ta) and B32 (Nb,W) separate at very low temperature, while the long-range ordered B2 (Mo,W;Nb,Ta) phase is stable up to roughly 600 K. For a detailed discussion on the impact of relaxation effects for this alloy and the consequences of its ordered phases, we refer to Ref. 50. It can be noted, however, that the Warren–Cowley parameters are not zero even at a relatively high temperature, revealing the presence of SRO in the solid solution regime ( $T > 600$  K).

Since it depends on the immediate chemical surrounding of an atom (typically the first three neighbor shells), SRO is a local property, difficult to capture experimentally. To compensate for this deficiency, different atomistic techniques were successfully applied to calculate SRO in HEAs. The most popular approaches involve Monte Carlo simulations on large supercells: these can be performed from first principles, but substantial computational resources are required to sample the whole configurational space and the possible supercell size is anyway restricted to a few hundreds of atoms. To overcome these limitations, classical or machine-learning potentials can be employed.<sup>50</sup> Alternatively, Ising Hamiltonians can be used, where the parameters describing the effective interactions can be fitted to a database of total energies,<sup>62</sup> constructed from a cluster expansion,<sup>63</sup> or calculated in a

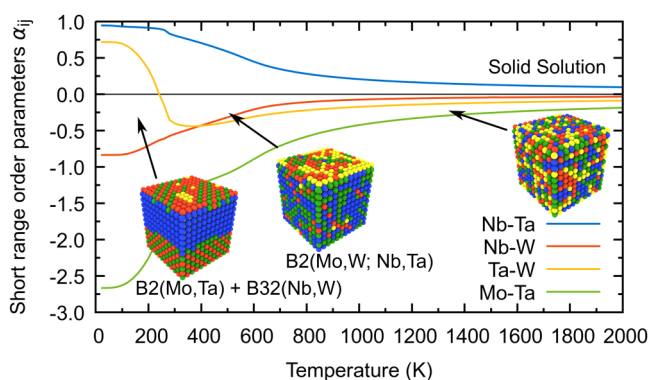


**FIG. 4.** Warren-Cowley short range order parameters as a function of temperature in MoNbTaW for four pairs of atoms. Adapted from Kostuchenko *et al.*, NPJ Comput. Mater. **5**, 55 (2019). Copyright 2019 Author(s), licensed under a Creative Commons Attribution (CC BY) license.

perturbative approach based on the coherent potential approximation, as proposed in the generalized perturbation method.<sup>64,65</sup> In contrast to Monte Carlo, within the analytical Concentration-wave approach,<sup>66</sup> the SRO parameters are evaluated in the reciprocal space. Ordering tendencies can be identified by particular “modes” corresponding to specific symmetric arrangements in real space revealing peaks at particular  $k$ -vectors.

Despite its local character, SRO can substantially impact the macroscopic properties of HEAs. The most obvious effect of SRO is on thermodynamic quantities and phase diagrams, and this was the focus of early works on SRO in HEAs.<sup>67,68</sup> More recently, however, it was realized by experiments and simulations that SRO affects deeply also the magnetic and mechanical properties of HEAs.

### A. SRO and magnetism

The interdependence between SRO and magnetism is critical in the alloys of the Cr-Mn-Fe-Co-Ni family. This family of alloys presents a peculiar magnetic situation in which ferromagnetic metals (Fe, Co, and Ni) and antiferromagnetic metals (Cr and Mn) are randomly mixed. The competing magnetic exchange interactions between atomic spins with different orientations may, however, result in magnetic frustration, which could prevent to realize energetically favorable configurations due to geometrical and chemical constraints. This is likely to produce a coupling between magnetic and chemical ordering as a result of this magnetic frustration, thereby leading to a preferential arrangement of atoms in the quinary alloy and some of its subsystems. Previous investigations already indicated the tendency toward ordering in binary alloys containing Cr and another magnetic metal.<sup>69–72</sup> For instance, a strong Cr-Cr repulsion at the nearest neighbor positions in Fe-Cr alloys was observed<sup>71,72</sup> and the analogous presence of SRO in Ni-Cr binary alloys<sup>69,70</sup> further suggests that similar ordering might also occur in several magnetic medium and high entropy alloys.

These observations for Cr-based alloys have led to several investigations on SRO in ternary CrCoNi and quaternary CrCoFeNi

alloys.<sup>65,73–77</sup> Tamm *et al.*<sup>73</sup> examined SRO in fcc CrCoNi using first-principles lattice Monte Carlo simulations. Their calculations at 500 K yielded Warren-Cowley parameters which deviated significantly from a random solid solution: the average number of Cr-Cr nearest neighbor pairs was reduced by  $\sim 40\%$ , whereas the number of Ni-Cr pairs was increased by  $\sim 25\%$ . The necessary energetic driving force for the SRO in this alloy is provided by the magnetic exchange interactions. For Cr atoms, the most preferred sites are second nearest neighbor sublattices with the parallel alignment of magnetic moments while Co atoms tend to have an antiparallel alignment of magnetic moments to those of neighboring Cr atoms.<sup>77</sup> In a random solid solution, the Cr magnetic moments have an irregular distribution of magnitude and direction originating from magnetic frustration. The structure with SRO, however, lowers this irregularity with most Cr atoms having magnetic moments close to  $\pm 2\mu_B$ .<sup>73</sup> Thus, the preferred arrangement of atoms triggered by magnetic exchange interactions reduces magnetic frustration and can lead to a lower energy state in this alloy.

Qualitatively similar trends of SRO as in the case of CrCoNi are also present in quaternary fcc CrCoFeNi.<sup>65,73,74,78</sup> Lattice Monte Carlo simulations at 500 K revealed a reduction of approximately 60% in the number of Cr-Cr nearest neighbor pairs, while a significant increase in the number of Co-Cr, Ni-Cr, and Ni-Fe pairs was found.<sup>73</sup> This suggests that the Cr atoms were ordered at the corner sites of a cubic sublattice. Based on *ab initio* calculations, Niu *et al.*<sup>74</sup> indeed demonstrated that the formation of a  $L1_2$  ordered phase, with Cr occupying the corner sites and rest of the atoms randomly mixed at the face centered sites, lowers the free energy as compared to a fully random solid solution. Additionally, Schönfeld *et al.*<sup>65</sup> recently calculated the effective pair interactions in this alloy with the Generalized Perturbation Method and used them subsequently in Monte Carlo simulations to predict an order-disorder transition at approximately 500 K. Their simulations yielded a strong interaction between Cr-Co and Cr-Ni nearest-neighbor pairs that originated from the electrostatic interaction between the atoms due to their size difference. The analysis of magnetic exchange interactions in the first coordination shell further revealed a dominant antiferromagnetic interaction between Cr and the rest of the atoms, whereas the interactions between Fe, Co, and Ni are mainly of the ferromagnetic type. Hence, the magnetic moments of Fe, Co, and Ni are usually aligned parallel, while Cr prefers an antiferromagnetic alignment to the ferromagnetic elements.<sup>74</sup> The spin-driven ordering of atoms in CrCoFeNi, similar to the CrCoNi alloy, thus avoids magnetic frustration and stabilizes the  $L1_2$  ordered phase.

Similar to Cr in this alloy class, the other antiferromagnetic element Mn also plays a pivotal role in determining the atomic ordering in HEAs. For example, recent *ab initio* calculations employing a conventional four-atom fcc unit cell within the coherent potential approximation predicted an antiferromagnetic ordering ( $\{100\}$  layered) for Mn atoms in some medium and high entropy alloys.<sup>79,80</sup> This antiferromagnetic ordering lowers the total energy with respect to the ferrimagnetic state, commonly chosen within single-atom calculations (see Fig. 5). Our own calculations showed that all magnetic elements in alloys with composition close to the equiatomic CrMnFeCoNi have a preference for some layered antiferromagnetic arrangement of magnetic moments, at least within the coherent potential approximation and assuming collinear ordering. Note that

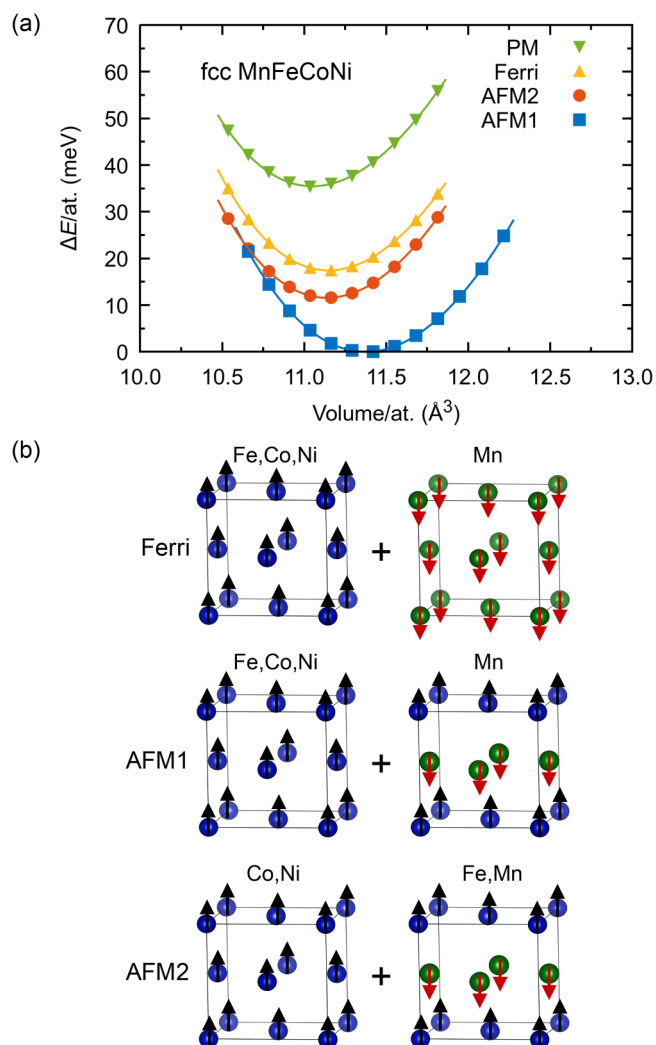


**FIG. 5.** (a) Total energy as a function of volume for paramagnetic (PM), ferromagnetic (Ferri), and two antiferromagnetic (AFM1 and AFM2) states of MnFeCoNi at 0 K. All total energies are referenced with respect to the total energy of the AFM1 state at its equilibrium volume. (b) The schematics of three different magnetic states. Adapted with permission from Rao *et al.*, Phys. Rev. Mater. 4, 014402 (2020). Copyright 2020 American Physical Society.

the initial configurations of local magnetic moments [Fig. 5(b)] were stable throughout the self-consistent calculations, i.e., no spin flips were observed. Interestingly, chemical SRO in CrMnFeCoNi, unlike for the ternary CrCoNi and quaternary CrCoFeNi alloys, has not yet been reported, a possible indication of the additional complexity introduced by the simultaneous presence of Cr and Mn.

Although the role of magnetism in magnetic HEAs can be significant as discussed above, the current understanding is still rather limited. The presence of multiple magnetic elements gives rise to complex scenarios, which are difficult to measure or simulate. For instance, strong magnetic ordering energies (which could

be anticipated for local environments rich in Fe, Co, or Ni, whose alloy derivatives have high Curie temperatures) may locally promote magnetic ordering and thus alter the overall phase stability. We thus anticipate that further improved predictions of these processes will be required to better address the interplay of magnetism, chemical ordering, and structural as well as functional properties of these multicomponent alloys.

## B. SRO and mechanical properties

SRO can change drastically the mechanical properties of fcc HEAs. Different local chemical arrangements have been observed to influence the stacking fault energy (SFE) in ternary, quaternary, and quinary alloys of the Cr-Mn-Fe-Co-Ni family,<sup>81–84</sup> to a degree that the SFE even qualitatively changes from negative to positive. Higher degrees of SRO generally increase the SFE, because favorable local arrangements must be broken to create a stacking fault, but exceptions cannot be excluded. Increasing the SFE in an fcc HEA can change the dominant deformation behavior from martensitic transformation to hcp (leading to transformation induced plasticity, TRIP) to formation of twins (twinning induced plasticity, TWIP) or simple dislocation slip. In general, it has been found that SRO also promotes local dislocation pinning and leads to strengthening.<sup>85,86</sup>

The effect of SRO on the mechanical properties has sparked a vivid debate, in particular, on the medium-entropy alloy CrCoNi that is worth to explore in detail. CrCoNi is one of the toughest known metallic alloys and its damage-tolerance even improves at low temperature.<sup>87</sup> As discussed in Sec. III A, SRO in this alloy is strongly influenced by magnetism, as Cr-Cr pairs tend to avoid magnetically frustrated configurations and thus appear repulsive in the first-neighbor shell. Ding *et al.*<sup>88</sup> proved with *ab initio* Monte Carlo simulations that SRO increases the SFE and the related energy difference between hcp and fcc in CrCoNi: starting from a random alloy, both these quantities were negative, i.e., the hcp phase of the alloy is thermodynamically more stable. Performing Monte Carlo simulations at 500 K, these values became positive, i.e., SRO stabilized the experimentally observed fcc phase. Li *et al.*<sup>85</sup> used a classical potential for the same alloy to show that SRO significantly modified the energy landscape and influenced the motion of dislocations. However, experiments performed by Yin *et al.*<sup>89</sup> demonstrated that the strength and hardness of CrCoNi samples prepared under different annealing conditions, and hence with presumably different degrees of SRO, were not affected by SRO. They therefore suggested that SRO would be non-negligible only for rather atypical low-temperature processing routes, which are not technologically relevant in practice. They also questioned the accuracy of first-principles calculations on CrCoNi by showing that misfit volumes, related to local atomic environments, are very poorly predicted by simulations. This critical position was though contradicted by a joint experimental-theoretical investigation,<sup>76</sup> in which SRO was detected by energy-filtered transition electron microscopy after aging at high temperature and strong evidence of its impact on dislocation motion and plasticity was revealed.

Based on these examples, one can expect that this exciting discussion will be soon also extended to other fcc HEAs of the Cr-Mn-Fe-Co-Ni family, while SRO was recently investigated also beyond this class of alloys.<sup>86,90</sup> As there is an ongoing debate

on the interpretation of very recent simulations and experiments, mainly due to the inherent technical difficulties involved in probing this subtle feature, we predict that the analysis of SRO will remain a very popular topic in future atomistic investigations of HEAs.

#### IV. NEW DEFECTS IN HEAs: INTERSTITIALS AND SURFACES

Early atomistic simulations of defects in HEAs analyzed either point defects (vacancies and self-interstitials) in an effort to explain the observed sluggish diffusion in some of the alloys<sup>91</sup> or extended defects involved in deformation (dislocations, stacking faults, twin boundaries) to provide an atomistic picture of the outstanding mechanical properties of these alloys. More recently, however, two new types of defects were considered: interstitial elements, which broaden the possibilities for materials design by considering off-lattice alloying and pave the way for efficient storage of gases, and surfaces, which extend the domain of application of HEAs to chemical reactions.

##### A. Interstitials

Interstitial alloying is a common approach to improve the mechanical properties of alloys and HEAs are no exception. The impact of alloying C in HEAs was investigated in several experimental studies<sup>92–102</sup> and, for the Cr-Mn-Fe-Co-Ni family, the addition of this element increased the yield and the ultimate strengths<sup>92,95,98–100</sup> while also impacting ductility.

For atomistic simulations, there are two challenges in the study of interstitial solutions in HEAs. First, since interstitial alloying induces significant lattice distortions around the interstitial atoms, typical mean-field approximations used to model HEAs (for example, the coherent potential approximation) usually cannot be employed directly, meaning that computationally more expensive supercell-based approaches need to be used. Second, the solution energy of interstitial atoms depends strongly on the local chemical environment, thus the computational cost of the simulations is also combinatorially high. For example, even taking into account only the first and the second nearest neighbor shells of the octahedral sites in the fcc structure (six and eight atoms, respectively), for a five-component system there are as many as  $5^{14}$  different atomic arrangements around an interstitial and considering them all is computationally intractable.

As mentioned above, due to the different chemical environments, the interstitial solution energy in a HEA does not take a single value, but is rather characterized by an almost continuous spectrum of different energies because of the large amount of possible local environments. Such a spectrum was calculated for the solution energies of C in the equiatomic CrMnFeCoNi alloy by sampling more than 1000 interstitial sites utilizing 20 supercell models with different atomic arrangements (Fig. 6).<sup>103</sup> The impact of C addition to CrMnFeCoNi was compared between the fcc and the hcp phases at 0 K and at finite temperature. It was found that the addition of C energetically destabilizes the hcp phase with respect to the fcc phase and thus increases the SFE in fcc CrMnFeCoNi, consistently with the experimental observation.<sup>100</sup>

The variation of the SFE with respect to the C content depends strongly on the constituent elements and the overall

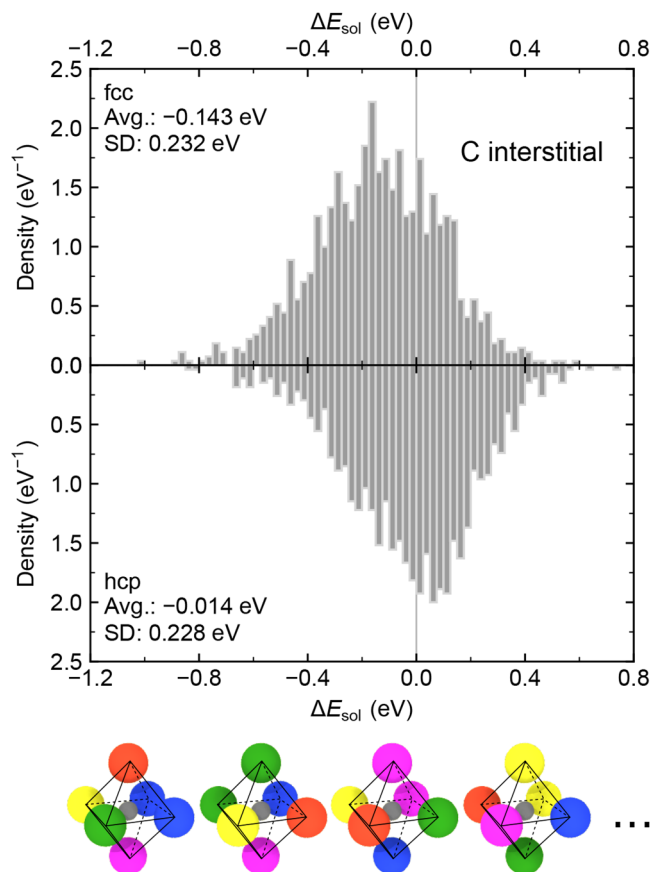


**FIG. 6.** Distribution of computed solution energies  $\Delta E_{\text{sol}}$  of interstitial C atoms at the octahedral sites in CrMnFeCoNi. The upper and the lower panels show the results for the fcc and the hcp phases, respectively. The average (avg.) and the standard deviation (SD) of  $\Delta E_{\text{sol}}$  are also shown in the panels. Reproduced with permission from Ikeda *et al.*, Phys. Rev. Mater. 3, 113603 (2019). Copyright 2019 American Physical Society.

composition of the considered HEA. A similar approach as above was applied to  $\text{Al}_{0.5}\text{MnFeCoNi}$ <sup>104</sup> and a decrease of the SFE was observed upon C addition, as confirmed also by experiments. However, this trend is reversed in the Al-free MnFeCoNi alloy, indicating that the reduction of the SFE in  $\text{Al}_{0.5}\text{MnFeCoNi}$  is driven mainly by the interaction between Al and C. These different trends demonstrate the potential of manipulating the impact of interstitial alloying to fine-tune the mechanical properties of HEAs.

Another application of interstitial alloying in HEAs is relevant for hydrogen storage.<sup>105–114</sup> The lattice distortions induced by chemical disorder and the quasi-continuous distribution of solution energies and volumes are believed to be the main reasons of high H-storage capability of some refractory HEAs. For example, Sahlberg *et al.*<sup>107</sup> observed a hydrogen content as high as 2.7 wt.% for TiVZrNbHf and it may be expected that, by replacing heavy elements like Hf with lighter ones, an even higher content of H (in

weight fraction) can be achieved. Hu *et al.*<sup>115</sup> studied the property of bcc ScTiZrMoHf as an H-storage material by both experiments and first-principles calculations. By analyzing the energy of more than 100 different configurations, the authors demonstrated that ScTiZrMoHf is stable with H content at least up to 2.14 wt.%, confirming the potential of this alloy as an H-storage material. Hu *et al.*<sup>116</sup> investigated TiZrNbMoHf with first-principles calculations and observed a bcc-fcc phase transition at high H content, in agreement with experimental findings.<sup>110</sup> They also discussed the relation between H solubility and lattice distortions and reported that lattice distortions in HEAs may enhance H solubility. At the present stage, atomistic simulations of HEAs as potential candidates for H storage are still in their infancy, but we foresee a blossoming of this field in the near future.

## B. Surfaces

Surfaces are another type of defect in HEAs that attracted the attention of the community only very recently. They determine the reactivity and response of metals to chemical substances and, in the context of HEAs, their properties are of interest for corrosion and heterogeneous catalysis.

Understanding corrosion in HEAs is crucial for two technological aspects. First, HEAs with high mechanical performance that endure harsh environments are desirable to extend the potential fields of application. Second, the composition of HEAs could be tailored to obtain high entropy coatings that maximize adherence and corrosion resistance to protect standard metals or other HEAs.

The corrosion resistance can often be improved by the addition of other elements to promote the formation of a passive layer, but relatively high concentrations of alloying elements are usually required (for example, almost 20% Cr is added to form stainless steels);<sup>118</sup> for HEAs, though, this would mean adding another element with a concentration comparable to the other components, possibly leading to modifications in the overall functionality of the alloy.

Atomistic simulations of HEAs related to corrosion mostly focused on oxidation, specifically on the bonding between the component elements in the alloys and O. In fact, different elements may have different interactions with O, leading either to segregation of one (or more) species to the surface or to complex absorption mechanisms if segregation is kinetically hindered. The trend of the binding energies  $E_{\text{bind}}$  between O and the metals in a HEA can be qualitatively described by the canonical Hammer-Nørskov theory,<sup>119</sup> for which  $E_{\text{bind}}$  anticorrelates to the baricenter of the  $d$ -band of the metal,

$$E_{\text{bind}} \propto - \frac{\int g_d(\epsilon)(\epsilon - \epsilon_F) d\epsilon}{\int g_d(\epsilon) d\epsilon}, \quad (5)$$

where  $g_d$  is the density of states for the  $d$ -valence electrons and  $\epsilon_F$  is the Fermi energy. For instance, in Cr-Mn-Fe-Co-Ni alloys, the elements Cr and Mn, with a high baricenter, bind more strongly to O, in agreement with Eq. (5) and thus tend to segregate to the surface; these elements actually form  $\text{Cr}_2\text{O}_3$  and  $\text{Mn}_2\text{O}_3$  oxides that partially protect from corrosion, with a mechanism similar to stainless steels.<sup>117</sup> In the refractory Mo-W-Ta-Ti-Zr HEAs, the binding energies of O on the surface follow the trend  $\text{Zr} < \text{Ti} < \text{Ta} < \text{Mo} < \text{W}$ ;

in this alloy, the binding of O with refractory HEAs is so strong that O is absorbed on the surface even at a pressure as low as  $10^{-9}$  atm and a temperature as high as 2000 K.<sup>120</sup>

The composition and structure of the surfaces of HEAs are very significant also for heterogeneous catalysis. Highly disordered configurations on the surface offer a broad variety of absorption sites with different binding energies for reactants and reaction intermediates and a higher chemical complexity increases the probability of occurrence of highly active sites. As the overall catalytic activity is dominated by the sites with the best absorption energy (the Sabatier principle), the overall composition of a candidate HEA catalysts can be tuned to maximize the number of sites with optimal binding energy, making them superior to any catalysts based on simple metals [Figs. 7(a) and 7(b)]. Ideally, other reaction intermediates could also be taken into account during this optimization process, potentially increasing the catalytic activity even further.

An issue that may impact the stability of HEA catalysts is surface segregation, because the larger number of components increases the likelihood of having large driving forces that pull or push certain elements to or from the surface. However, very weak

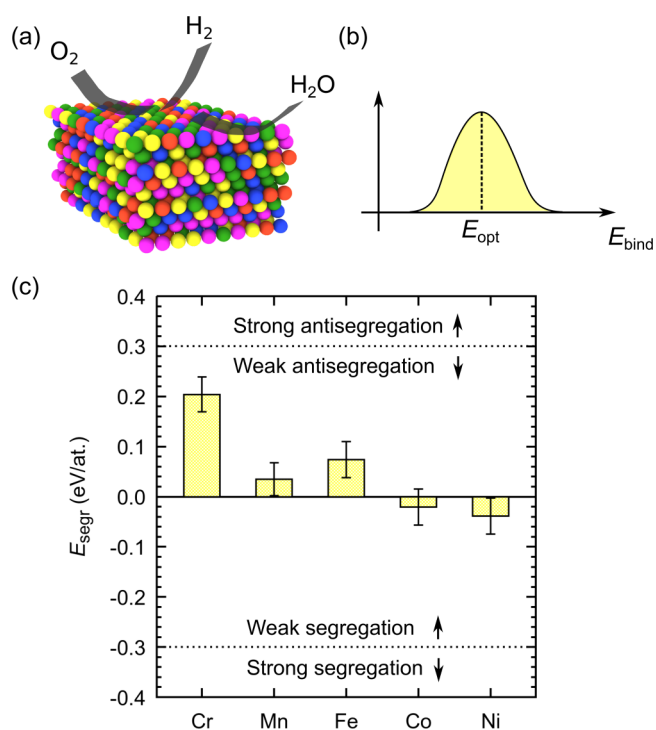


**FIG. 7.** (a) Schematics of a possible chemical reaction catalyzed by a quinary HEA, assuming that surface segregation does not take place. (b) The composition of the alloy can be tuned so that the distribution of binding energy peaks at the optimal absorption energy for one or more reactants. (c) Surface segregation energies of the component elements in CrMnFeCoNi. The calculation setup is detailed in Ref. 117. Statistical error bars due to the different atomic environments are indicated.

segregation was so far observed in simulations under non-reactive conditions for Co-Mo-Fe-Ni-Cu<sup>121</sup> and Co-Ir-Ni-Ru-Rh,<sup>122</sup> hinting that a disordered configuration of these particular alloys may be stable even at relatively low temperature. For Cr-Mn-Fe-Co-Ni, *ab initio* calculations<sup>117</sup> also suggest that the segregation is weak, especially if compared to common bimetallic alloys: for instance, as shown in Fig. 7(c), the surface segregation energies of the single elements in CrMnFeCoNi are relatively small in magnitude ( $-0.3\text{ eV} < E_{\text{segr}} < 0.3\text{ eV}$ ). Monte Carlo simulations with a modified embedded atom potential,<sup>123</sup> however, pointed out a somewhat stronger segregation of Mn in CrMnFeCoNi, presumably a consequence of the low surface formation energy of Mn predicted by that particular potential. Although the presence of molecules at the surface severely enhances segregation, this is expected to be hindered by slow diffusion and HEA catalysts should be able to retain a metastable disordered configuration also when exposed to the reactants.

A combination of first principles calculations and machine learning for the quinary HEAs Ir-Pd-Pt-Rh-Ru, Co-Cu-Ga-Ni-Zn, and Ag-Au-Cu-Pd-Pt was employed to guide the discovery of new catalysts for the O<sub>2</sub>, CO<sub>2</sub>, and CO reduction reactions:<sup>124,125</sup> for these alloys, a database of absorption energies for different permutations of the elements surrounding the adsorbed molecule was fitted using as descriptors the chemical identities of the atoms in the first three neighbor shells around the adsorbate. The obtained model was then used to determine the best composition by maximizing the occurrence of sites with a predefined optimal absorption energy, leading to a significant increase of the computed catalytic activity.

HEA catalysts look so promising that they were even designated as “paradigm-shifting” discoveries for heterogeneous catalysis.<sup>126</sup> Given the novelty of this particular research direction for HEAs, the structure, composition, and properties of the surfaces of HEAs are still largely unexplored from both experiments and simulations.<sup>127</sup> Nevertheless, the prospect for diverse technological applications is currently clearly attracting the attention of a rapidly growing community of material scientists, chemists, and physicists in this field.

## V. CONCLUSIONS AND OUTLOOK

HEAs have quickly evolved to one of the most important research fields in materials science. First mainly explored experimentally, atomistic simulations of these alloys have now entered a golden age as well. In this Perspective, we commented on three aspects that significantly advanced the field of atomistic simulations of HEAs only very recently: the introduction of machine-learning potentials, which provided unprecedented accuracy in the calculation of thermodynamic properties; the analysis of short-range order, which improved the approximation of a random lattice and can couple to macroscopic properties; and the study of interstitials and surfaces, which greatly extended the domain of application of HEAs to hydrogen storage or heterogeneous catalysis, or enhanced even more the mechanical properties.

The future of atomistic simulations of HEAs looks more and more intimately connected with the concept of materials design and the three highlights presented here will likely be key approaches to discover new HEAs with better properties. In

particular, machine learning potentials can advance the understanding of phase stabilities, ultimately leading to the construction of complete phase diagrams for these alloys; SRO can be controlled experimentally by different processing routes to adjust the relative occurrence of specific atomic arrangements and even obtain a tailored distribution of atoms; complex defects can be introduced to achieve multifunctional alloys optimized for more than one task or condition, which are particularly appealing in the context of sustainability.

The chemical complexity and the generality of the concept of HEAs so far encouraged innovation in the form of extension of standard techniques, and out-of-the-box thinking in the form of creation of new research paths. As the HEA community is rapidly expanding, we anticipate that many more original and exciting methods will be developed in upcoming years, not only advancing our understanding of this particular alloy class, but lifting the simulation tools for various materials design aspects and broader applicability to a new level.

## ACKNOWLEDGMENTS

A.F., B.D., K.G., P.S., and F.K. acknowledge funding from Nederlandse Organisatie voor Wetenschappelijk Onderzoek (NWO) / Stichting voor de Technische Wetenschappen (STW), VIDI Grant No. 15707. Y.I. and B.G. acknowledge funding from Deutsche Forschungsgemeinschaft (DFG), Research Project No. GR 3716/5-1, and European Research Council (ERC) under the EU's Horizon 2020 research and innovation programme, Grant Agreement No. 639211.

## DATA AVAILABILITY

Data sharing is not applicable to this article as no new data were created or analyzed in this study.

## REFERENCES

- <sup>1</sup>J.-W. Yeh, S.-K. Chen, S.-J. Lin, J.-Y. Gan, T.-S. Chin, T.-T. Shun, C.-H. Tsau, and S.-Y. Chang, “Nanostructured high-entropy alloys with multiple principal elements: Novel alloy design concepts and outcomes,” *Adv. Eng. Mater.* **6**, 299–303 (2004).
- <sup>2</sup>B. Cantor, I. T. H. Chang, P. Knight, and A. J. B. Vincent, “Microstructural development in equiatomic multicomponent alloys,” *Mater. Sci. Eng. A* **375**, 213–218 (2004).
- <sup>3</sup>B. S. Murty, J.-W. Yeh, S. Ranganathan, and P. P. Bhattacharjee, *High-Entropy Alloys* (Elsevier, 2019).
- <sup>4</sup>O. N. Senkov, G. B. Wilks, J. M. Scott, and D. B. Miracle, “Mechanical properties of Nb<sub>25</sub>Mo<sub>25</sub>Ta<sub>25</sub>W<sub>25</sub> and V<sub>20</sub>Nb<sub>20</sub>Mo<sub>20</sub>Ta<sub>20</sub>W<sub>20</sub> refractory high entropy alloys,” *Intermetallics* **19**, 698–706 (2011).
- <sup>5</sup>A. Gali and E. P. George, “Tensile properties of high-and medium-entropy alloys,” *Intermetallics* **39**, 74–78 (2013).
- <sup>6</sup>F. Otto, A. Dlouhý, C. Somsen, H. Bei, G. Eggeler, and E. P. George, “The influences of temperature and microstructure on the tensile properties of a CoCrFeMnNi high-entropy alloy,” *Acta Mater.* **61**, 5743–5755 (2013).
- <sup>7</sup>B. Gludovatz, A. Hohenwarter, D. Catoor, E. H. Chang, E. P. George, and R. O. Ritchie, “A fracture-resistant high-entropy alloy for cryogenic applications,” *Science* **345**, 1153–1158 (2014).
- <sup>8</sup>D. B. Miracle, J. D. Miller, O. N. Senkov, C. Woodward, M. D. Uchic, and J. Tiley, “Exploration and development of high entropy alloys for structural applications,” *Entropy* **16**, 494–525 (2014).

- <sup>9</sup>B. Gludovatz, E. P. George, and R. O. Ritchie, "Processing, microstructure and mechanical properties of the CrMnFeCoNi high-entropy alloy," *JOM* **67**, 2262–2270 (2015).
- <sup>10</sup>D. B. Miracle and O. N. Senkov, "A critical review of high entropy alloys and related concepts," *Acta Mater.* **122**, 448–511 (2017).
- <sup>11</sup>P. Sarker, T. Harrington, C. Toher, C. Oses, M. Samiee, J.-P. Maria, D. W. Brenner, K. S. Vecchio, and S. Curtarolo, "High-entropy high-hardness metal carbides discovered by entropy descriptors," *Nat. Commun.* **9**, 1–10 (2018).
- <sup>12</sup>F. Otto, A. Dlouhý, K. G. Pradeep, M. Kuběnová, D. Raabe, G. Eggeler, and E. P. George, "Decomposition of the single-phase high-entropy alloy CrMnFeCoNi after prolonged anneals at intermediate temperatures," *Acta Mater.* **112**, 40–52 (2016).
- <sup>13</sup>Y. Ikeda, B. Grabowski, and F. Körmann, "Ab initio phase stabilities and mechanical properties of multicomponent alloys: A comprehensive review for high entropy alloys and compositionally complex alloys," *Mater. Charact.* **147**, 464–511 (2019).
- <sup>14</sup>Z. H. Aitken, V. Sorkin, and Y.-W. Zhang, "Atomistic modeling of nanoscale plasticity in high-entropy alloys," *J. Mater. Res.* **34**, 1509–1532 (2019).
- <sup>15</sup>J. Rickman, H. Chan, M. Harmer, J. Smeltzer, C. Marvel, A. Roy, and G. Balasubramanian, "Materials informatics for the screening of multi-principal elements and high-entropy alloys," *Nat. Commun.* **10**, 1–10 (2019).
- <sup>16</sup>Y. Li and W. Guo, "Machine-learning model for predicting phase formations of high-entropy alloys," *Phys. Rev. Mater.* **3**, 095005 (2019).
- <sup>17</sup>N. Qu, Y. Chen, Z. Lai, Y. Liu, and J. Zhu, "The phase selection via machine learning in high entropy alloys," *Procedia Manuf.* **37**, 299–305 (2019).
- <sup>18</sup>A. Agarwal and A. P. Rao, "Artificial intelligence predicts body-centered-cubic and face-centered-cubic phases in high-entropy alloys," *JOM* **71**, 3424–3432 (2019).
- <sup>19</sup>Y. Zhang, C. Wen, C. Wang, S. Antonov, D. Xue, Y. Bai, and Y. Su, "Phase prediction in high entropy alloys with a rational selection of materials descriptors and machine learning models," *Acta Mater.* **185**, 528–539 (2020).
- <sup>20</sup>Z. Pei, J. Yin, J. A. Hawk, D. E. Alman, and M. C. Gao, "Machine-learning informed prediction of high-entropy solid solution formation: Beyond the Hume-Rothery rules," *NPJ Comput. Mater.* **6**, 1–8 (2020).
- <sup>21</sup>K. C. Pitike, K. C. Santosh, M. Eisenbach, C. A. Bridges, and V. R. Cooper, "Predicting the phase stability of multi-component high entropy compounds," *Chem. Mater.* **32**, 7507–7515 (2020).
- <sup>22</sup>C. Oses, C. Toher, and S. Curtarolo, "High-entropy ceramics," *Nat. Rev. Mater.* **5**, 295–309 (2020).
- <sup>23</sup>S. Manzhos and T. Carrington, Jr., "A random-sampling high dimensional model representation neural network for building potential energy surfaces," *J. Chem. Phys.* **125**, 084109 (2006).
- <sup>24</sup>J. Behler and M. Parrinello, "Generalized neural-network representation of high-dimensional potential-energy surfaces," *Phys. Rev. Lett.* **98**, 146401 (2007).
- <sup>25</sup>A. P. Bartók, M. C. Payne, R. Kondor, and G. Csányi, "Gaussian approximation potentials: The accuracy of quantum mechanics, without the electrons," *Phys. Rev. Lett.* **104**, 136403 (2010).
- <sup>26</sup>M. Rupp, A. Tkatchenko, K.-R. Müller, and O. A. Von Lilienfeld, "Fast and accurate modeling of molecular atomization energies with machine learning," *Phys. Rev. Lett.* **108**, 058301 (2012).
- <sup>27</sup>Z. Li, J. R. Kermode, and A. De Vita, "Molecular dynamics with on-the-fly machine learning of quantum-mechanical forces," *Phys. Rev. Lett.* **114**, 096405 (2015).
- <sup>28</sup>A. P. Thompson, L. P. Swiler, C. R. Trott, S. M. Foiles, and G. J. Tucker, "Spectral neighbor analysis method for automated generation of quantum-accurate interatomic potentials," *J. Comput. Phys.* **285**, 316–330 (2015).
- <sup>29</sup>A. V. Shapeev, "Moment tensor potentials: A class of systematically improvable interatomic potentials," *Multiscale Model. Simul.* **14**, 1153–1173 (2016).
- <sup>30</sup>N. Artrith, A. Urban, and G. Ceder, "Efficient and accurate machine-learning interpolation of atomic energies in compositions with many species," *Phys. Rev. B* **96**, 014112 (2017).
- <sup>31</sup>R. Drautz, "Atomic cluster expansion for accurate and transferable interatomic potentials," *Phys. Rev. B* **99**, 014104 (2019).
- <sup>32</sup>S. Curtarolo, W. Setyawan, G. L. Hart, M. Jahnatek, R. V. Chepulskii, R. H. Taylor, S. Wang, J. Xue, K. Yang, O. Levy *et al.*, "AFLOW: An automatic framework for high-throughput materials discovery," *Comput. Mater. Sci.* **58**, 218–226 (2012).
- <sup>33</sup>R. Ramakrishnan, P. O. Dral, M. Rupp, and O. A. Von Lilienfeld, "Quantum chemistry structures and properties of 134 kilo molecules," *Sci. Data* **1**, 1–7 (2014).
- <sup>34</sup>S. P. Ong, S. Cholia, A. Jain, M. Brafman, D. Gunter, G. Ceder, and K. A. Persson, "The materials application programming interface (API): A simple, flexible and efficient API for materials data based on REpresentational state transfer (REST) principles," *Comput. Mater. Sci.* **97**, 209–215 (2015).
- <sup>35</sup>C. Draxl and M. Scheffler, "The NOMAD laboratory: From data sharing to artificial intelligence," *J. Phys. Mater.* **2**, 036001 (2019).
- <sup>36</sup>N. Artrith and J. Behler, "High-dimensional neural network potentials for metal surfaces: A prototype study for copper," *Phys. Rev. B* **85**, 045439 (2012).
- <sup>37</sup>J. S. Smith, B. Nebgen, N. Lubbers, O. Isayev, and A. E. Roitberg, "Less is more: Sampling chemical space with active learning," *J. Chem. Phys.* **148**, 241733 (2018).
- <sup>38</sup>R. Jinnouchi, F. Karsai, and G. Kresse, "On-the-fly machine learning force field generation: Application to melting points," *Phys. Rev. B* **100**, 014105 (2019).
- <sup>39</sup>E. Uteva, R. S. Graham, R. D. Wilkinson, and R. J. Wheatley, "Active learning in Gaussian process interpolation of potential energy surfaces," *J. Chem. Phys.* **149**, 174114 (2018).
- <sup>40</sup>J. Vandermause, S. B. Torrisi, S. Batzner, Y. Xie, L. Sun, A. M. Kolpak, and B. Kozinsky, "On-the-fly active learning of interpretable Bayesian force fields for atomistic rare events," *NPJ Comput. Mater.* **6**, 1–11 (2020).
- <sup>41</sup>A. P. Bartók, R. Kondor, and G. Csányi, "On representing chemical environments," *Phys. Rev. B* **87**, 184115 (2013).
- <sup>42</sup>E. V. Podryabinkin and A. V. Shapeev, "Active learning of linearly parameterized interatomic potentials," *Comput. Mater. Sci.* **140**, 171–180 (2017).
- <sup>43</sup>A. Glensk, B. Grabowski, and T. H. annd J. Neugebauer, "Understanding anharmonicity in fcc materials: From its origin to ab initio strategies beyond the quasiharmonic approximation," *Phys. Rev. Lett.* **114**, 195901 (2015).
- <sup>44</sup>X. Zhang, B. Grabowski, F. Körmann, A. V. Ruban, Y. Gong, R. C. Reed, T. Hicke, and J. Neugebauer, "Temperature dependence of the stacking-fault gibbs energy for Al, Cu and Ni," *Phys. Rev. B* **98**, 224106 (2018).
- <sup>45</sup>B. Grabowski, Y. Ikeda, P. Srinivasan, F. Körmann, C. Freysoldt, A. I. Duff, A. Shapeev, and J. Neugebauer, "Ab initio vibrational free energies including anharmonicity for multicomponent alloys," *NPJ Comput. Mater.* **5**, 1–6 (2019).
- <sup>46</sup>A. I. Duff, T. Davey, D. Korbmayer, A. Glensk, B. Grabowski, J. Neugebauer, and M. W. Finnis, "Improved method of calculating ab initio high-temperature thermodynamic properties with application to ZrC," *Phys. Rev. B* **91**, 214311 (2015).
- <sup>47</sup>M. S. Daw and M. I. Baskes, "Semiempirical, quantum mechanical calculation of hydrogen embrittlement in metals," *Phys. Rev. Lett.* **50**, 1285 (1983).
- <sup>48</sup>M. W. Finnis and J. E. Sinclair, "A simple empirical n-body potential for transition metals," *Philos. Mag. A* **50**, 45–55 (1984).
- <sup>49</sup>A. Shapeev, "Accurate representation of formation energies of crystalline alloys with many components," *Comput. Mater. Sci.* **139**, 26–30 (2017).
- <sup>50</sup>T. Kostuchenko, F. Körmann, J. Neugebauer, and A. Shapeev, "Impact of lattice relaxations on phase transitions in a high-entropy alloy studied by machine-learning potentials," *NPJ Comput. Mater.* **5**, 1–7 (2019).
- <sup>51</sup>E. Meshkov, I. Novoselov, A. Shapeev, and A. Yanilkin, "Sublattice formation in CoCrFeNi high-entropy alloy," *Intermetallics* **112**, 106542 (2019).
- <sup>52</sup>I. Balyakin, A. Yuryev, B. Gelchinski, and A. Rempel, "Ab initio molecular dynamics and high-dimensional neural network potential study of VZrNbHfTa melt," *J. Phys. Condens. Matter* **32**, 214006 (2020).
- <sup>53</sup>M. Jafary-Zadeh, K. H. Khoo, R. Laskowski, P. S. Branicio, and A. V. Shapeev, "Applying a machine learning interatomic potential to unravel the effects of local lattice distortion on the elastic properties of multi-principal element alloys," *J. Alloys Compd.* **803**, 1054–1062 (2019).

- <sup>54</sup>P. Soven, "Coherent-potential model of substitutional disordered alloys," *Phys. Rev.* **156**, 809 (1967).
- <sup>55</sup>B. Gyorffy, "Coherent-potential approximation for a nonoverlapping-muffin-tin-potential model of random substitutional alloys," *Phys. Rev. B* **5**, 2382 (1972).
- <sup>56</sup>A. Zunger, S.-H. Wei, L. Ferreira, and J. E. Bernard, "Special quasirandom structures," *Phys. Rev. Lett.* **65**, 353 (1990).
- <sup>57</sup>S.-H. Wei, L. G. Ferreira, J. E. Bernard, and A. Zunger, "Electronic properties of random alloys: Special quasirandom structures," *Phys. Rev. B* **42**, 9622 (1990).
- <sup>58</sup>C. Jiang and B. P. Uberuaga, "Efficient ab initio modeling of random multi-component alloys," *Phys. Rev. Lett.* **116**, 105501 (2016).
- <sup>59</sup>P. Yu, J.-P. Chou, Y.-C. Lo, and A. Hu, "An optimized random structures generator governed by chemical short-range order for multi-component solid solutions," *Model. Simul. Mater. Sci. Eng.* **27**, 085007 (2019).
- <sup>60</sup>J. Cowley, "An approximate theory of order in alloys," *Phys. Rev.* **77**, 669 (1950).
- <sup>61</sup>N. Norman and B. E. Warren, "X-ray measurement of short range order in Ag-Au," *J. Appl. Phys.* **22**, 483–486 (1951).
- <sup>62</sup>J. Zhang, X. Liu, S. Bi, J. Yin, G. Zhang, and M. Eisenbach, "Robust data-driven approach for predicting the configurational energy of high entropy alloys," *Mater. Des.* **185**, 108247 (2020).
- <sup>63</sup>J. M. Sanchez, F. Ducastelle, and D. Gratias, "Generalized cluster description of multicomponent systems," *Physica A* **128**, 334–350 (1984).
- <sup>64</sup>F. Ducastelle and F. Gautier, "Generalized perturbation theory in disordered transitional alloys: Applications to the calculation of ordering energies," *J. Phys. F Met. Phys.* **6**, 2039 (1976).
- <sup>65</sup>B. Schönfeld, C. R. Sax, J. Zemp, M. Engelke, P. Boesecke, T. Kresse, T. Boll, T. Al-Kassab, O. E. Peil, and A. V. Ruban, "Local order in Cr-Fe-Co-Ni: Experiment and electronic structure calculations," *Phys. Rev. B* **99**, 014206 (2019).
- <sup>66</sup>P. Singh, A. V. Smirnov, and D. D. Johnson, "Atomic short-range order and incipient long-range order in high-entropy alloys," *Phys. Rev. B* **91**, 224204 (2015).
- <sup>67</sup>M. Widom, W. P. Huhn, S. Maiti, and W. Steurer, "Hybrid Monte Carlo/molecular dynamics simulation of a refractory metal high entropy alloy," *Metall. Mater. Trans. A* **45**, 196–200 (2014).
- <sup>68</sup>F. Körmann, A. V. Ruban, and M. H. Sluiter, "Long-ranged interactions in bcc NbMoTaW high-entropy alloys," *Mater. Res. Lett.* **5**, 35–40 (2017).
- <sup>69</sup>W. Schweika and H.-G. Haubold, "Neutron-scattering and Monte Carlo study of short-range order and atomic interaction in  $\text{Ni}_{0.89}\text{Cr}_{0.11}$ ," *Phys. Rev. B* **37**, 9240 (1988).
- <sup>70</sup>B. Schönfeld, L. Reinhard, G. Kosterz, and W. Bührer, "Short-range order and atomic displacements in Ni-20 at.% Cr single crystals," *Phys. Status Solidi B* **148**, 457–471 (1988).
- <sup>71</sup>T. P. C. Klaver, R. Drautz, and M. W. Finnis, "Magnetism and thermodynamics of defect-free Fe-Cr alloys," *Phys. Rev. B* **74**, 094435 (2006).
- <sup>72</sup>A. Caro, M. Caro, P. Klaver, B. Sadigh, E. Lopasso, and S. Srinivasan, "The computational modeling of alloys at the atomic scale: From ab initio and thermodynamics to radiation-induced heterogeneous precipitation," *JOM* **59**, 52–57 (2007).
- <sup>73</sup>A. Tamm, A. Aabloo, M. Klintonberg, M. Stocks, and A. Caro, "Atomic-scale properties of Ni-based fcc ternary, and quaternary alloys," *Acta Mater.* **99**, 307–312 (2015).
- <sup>74</sup>C. Niu, A. Zaddach, A. Oni, X. Sang, J. Hurt III, J. LeBeau, C. Koch, and D. Irving, "Spin-driven ordering of Cr in the equiatomic high entropy alloy NiFeCrCo," *Appl. Phys. Lett.* **106**, 161906 (2015).
- <sup>75</sup>C. Niu, C. R. LaRosa, J. Miao, M. J. Mills, and M. Ghazisaeidi, "Magnetically-driven phase transformation strengthening in high entropy alloys," *Nat. Commun.* **9**, 1–9 (2018).
- <sup>76</sup>R. Zhang, S. Zhao, J. Ding, Y. Chong, T. Jia, C. Ophus, M. Asta, R. O. Ritchie, and A. M. Minor, "Short-range order and its impact on the CrCoNi medium-entropy alloy," *Nature* **581**, 283–287 (2020).
- <sup>77</sup>F. Walsh, R. O. Ritchie, and M. Asta, "Interdependence of magnetic and chemical short-range order in the CrCoNi multi-principal element alloy," *arXiv:2004.09086* (2020).
- <sup>78</sup>T. Fukushima, H. Katayama-Yoshida, K. Sato, M. Ogura, R. Zeller, and P. H. Dederichs, "Local energies and energy fluctuations—Applied to the high entropy alloy CrFeCoNi," *J. Phys. Soc. Jpn.* **86**, 114704 (2017).
- <sup>79</sup>S. Mu, J. Yin, G. D. Samolyuk, S. Wimmer, Z. Pei, M. Eisenbach, S. Mankovsky, H. Ebert, and G. M. Stocks, "Hidden Mn magnetic-moment disorder and its influence on the physical properties of medium-entropy NiCoMn solid solution alloys," *Phys. Rev. Mater.* **3**, 014411 (2019).
- <sup>80</sup>Z. Rao, B. Dutta, F. Körmann, D. Ponge, L. Li, J. He, L. Stephenson, L. Schäfer, K. Skokov, O. Gutfleisch, D. Raabe, and Z. Li, "Unveiling the mechanism of abnormal magnetic behavior of fcc high-entropy alloys through a joint experimental-theoretical study," *Phys. Rev. Mater.* **4**, 014402 (2020).
- <sup>81</sup>Y. H. Zhang, Y. Zhuang, A. Hu, J.-J. Kai, and C. T. Liu, "The origin of negative stacking fault energies and nano-twin formation in face-centered cubic high entropy alloys," *Scr. Mater.* **130**, 96–99 (2017).
- <sup>82</sup>Y. Ikeda, F. Körmann, I. Tanaka, and J. Neugebauer, "Impact of chemical fluctuations on stacking fault energies of CrCoNi and CrMnFeCoNi high entropy alloys from first principles," *Entropy* **20**, 655 (2018).
- <sup>83</sup>S. Zhao, Y. Osetsky, G. M. Stocks, and Y. Zhang, "Local-environment dependence of stacking fault energies in concentrated solid-solution alloys," *NPJ Comput. Mater.* **5**, 1–7 (2019).
- <sup>84</sup>X. Wu, Z. Li, Z. Rao, Y. Ikeda, B. Dutta, F. Körmann, J. Neugebauer, and D. Raabe, "Role of magnetic ordering for the design of quinary twip-trip high entropy alloys," *Phys. Rev. Mater.* **4**, 033601 (2020).
- <sup>85</sup>Q.-J. Li, H. Sheng, and E. Ma, "Strengthening in multi-principal element alloys with local-chemical-order roughened dislocation pathways," *Nat. Commun.* **10**, 1–11 (2019).
- <sup>86</sup>E. Antillon, C. Woodward, S. I. Rao, B. Akdim, and T. Parthasarathy, "Chemical short range order strengthening in a model fcc high entropy alloy," *Acta Mater.* **190**, 29–42 (2020).
- <sup>87</sup>B. Gludovatz, A. Hohenwarter, K. V. Thurston, H. Bei, Z. Wu, E. P. George, and R. O. Ritchie, "Exceptional damage-tolerance of a medium-entropy alloy CrCoNi at cryogenic temperatures," *Nat. Commun.* **7**, 1–8 (2016).
- <sup>88</sup>J. Ding, Q. Yu, M. Asta, and R. O. Ritchie, "Tunable stacking fault energies by tailoring local chemical order in CrCoNi medium-entropy alloys," *PNAS* **115**, 8919–8924 (2018).
- <sup>89</sup>B. Yin, S. Yoshida, N. Tsuji, and W. A. Curtin, "Yield strength and misfit volumes of NiCoCr and implications for short-range-order," *Nat. Commun.* **11**, 1–7 (2020).
- <sup>90</sup>S. Yin, J. Ding, M. Asta, and R. O. Ritchie, "Ab initio modeling of the role of local chemical short-range order on the Peierls potential of screw dislocations in body-centered cubic high-entropy alloys," *NPJ Comput. Mater.* **6**, 1–11 (2020).
- <sup>91</sup>K.-Y. Tsai, M.-H. Tsai, and J.-W. Yeh, "Sluggish diffusion in Co-Cr-Fe-Mn-Ni high-entropy alloys," *Acta Mater.* **61**, 4887–4897 (2013).
- <sup>92</sup>Z. Wu, C. Parish, and H. Bei, "Nano-twin mediated plasticity in carbon-containing FeNiCoCrMn high entropy alloys," *J. Alloys Compd.* **647**, 815–822 (2015).
- <sup>93</sup>Z. Wang, I. Baker, Z. Cai, S. Chen, J. D. Poplawsky, and W. Guo, "The effect of interstitial carbon on the mechanical properties and dislocation substructure evolution in  $\text{Fe}_{40.4}\text{Ni}_{11.3}\text{Mn}_{34.8}\text{Al}_{7.5}\text{Cr}_6$  high entropy alloys," *Acta Mater.* **120**, 228–239 (2016).
- <sup>94</sup>Z. Wang and I. Baker, "Interstitial strengthening of a f.c.c. FeNiMnAlCr high entropy alloy," *Mater. Lett.* **180**, 153–156 (2016).
- <sup>95</sup>Z. Li, C. C. Tasan, H. Springer, B. Gault, and D. Raabe, "Interstitial atoms enable joint twinning and transformation induced plasticity in strong and ductile high-entropy alloys," *Sci. Rep.* **7**, 40704 (2017).
- <sup>96</sup>Z. Wang, I. Baker, W. Guo, and J. D. Poplawsky, "The effect of carbon on the microstructures, mechanical properties, and deformation mechanisms of thermo-mechanically treated  $\text{Fe}_{40.4}\text{Ni}_{11.3}\text{Mn}_{34.8}\text{Al}_{7.5}\text{Cr}_6$  high entropy alloys," *Acta Mater.* **126**, 346–360 (2017).

- <sup>97</sup>H. Luo, Z. Li, W. Lu, D. Ponge, and D. Raabe, "Hydrogen embrittlement of an interstitial equimolar high-entropy alloy," *Corros. Sci.* **136**, 403–408 (2018).
- <sup>98</sup>J. Chen, Z. Yao, X. Wang, Y. Lu, X. Wang, Y. Liu, and X. Fan, "Effect of C content on microstructure and tensile properties of as-cast CoCrFeMnNi high entropy alloy," *Mater. Chem. Phys.* **210**, 136–145 (2018).
- <sup>99</sup>L. Chen, R. Wei, K. Tang, J. Zhang, F. Jiang, L. He, and J. Sun, "Heavy carbon alloyed fcc-structured high entropy alloy with excellent combination of strength and ductility," *Mater. Sci. Eng. A* **716**, 150–156 (2018).
- <sup>100</sup>Z. Li, "Interstitial equiatomic CoCrFeMnNi high-entropy alloys: Carbon content, microstructure, and compositional homogeneity effects on deformation behavior," *Acta Mater.* **164**, 400–412 (2019).
- <sup>101</sup>Y. Shang, Y. Wu, J. He, X. Zhu, S. Liu, H. Huang, K. An, Y. Chen, S. Jiang, H. Wang, X. Liu, and Z. Lu, "Solving the strength-ductility tradeoff in the medium-entropy NiCoCr alloy via interstitial strengthening of carbon," *Intermetallics* **106**, 77–87 (2019).
- <sup>102</sup>M. Wu, Z. Li, B. Gault, P. Munroe, and I. Baker, "The effects of carbon on the phase stability and mechanical properties of heat-treated FeNiMnCrAl high entropy alloys," *Mater. Sci. Eng. A* **748**, 59–73 (2019).
- <sup>103</sup>Y. Ikeda, I. Tanaka, J. Neugebauer, and F. Körmann, "Impact of interstitial C on phase stability and stacking-fault energy of the CrMnFeCoNi high-entropy alloy," *Phys. Rev. Mater.* **3**, 113603 (2019).
- <sup>104</sup>F. Kies, Y. Ikeda, S. Ewald, J. H. Schleifenbaum, B. Hallstedt, F. Körmann, and C. Haase, "Combined Al and C alloying enables mechanism-oriented design of multi-principal element alloys: Ab initio calculations and experiments," *Scr. Mater.* **178**, 366–371 (2020).
- <sup>105</sup>Y.-F. Kao, S.-K. Chen, J.-H. Sheu, J.-T. Lin, W.-E. Lin, J.-W. Yeh, S.-J. Lin, T.-H. Liou, and C.-W. Wang, "Hydrogen storage properties of multi-principal-component CoFeMnTi<sub>x</sub>V<sub>y</sub>Zr<sub>z</sub> alloys," *Int. J. Hydrogen Energy* **35**, 9046–9059 (2010).
- <sup>106</sup>I. Kunce, M. Polanski, and J. Bystrzycki, "Structure and hydrogen storage properties of a high entropy ZrTiVCrFeNi alloy synthesized using laser engineered net shaping (LENS)," *Int. J. Hydrogen Energy* **38**, 12180–12189 (2013).
- <sup>107</sup>M. Sahlberg, D. Karlsson, C. Zlotea, and U. Jansson, "Superior hydrogen storage in high entropy alloys," *Sci. Rep.* **6**, 36770 (2016).
- <sup>108</sup>D. Karlsson, G. Ek, J. Cedervall, C. Zlotea, K. T. Möller, T. C. Hansen, J. Bednarcík, M. Paskevicius, M. H. Sorby, T. R. Jensen, U. Jansson, and M. Sahlberg, "Structure and hydrogenation properties of a HfNbTiVZr high-entropy alloy," *Inorg. Chem.* **57**, 2103–2110 (2018).
- <sup>109</sup>M. M. Nygård, G. Ek, D. Karlsson, M. H. Sorby, M. Sahlberg, and B. C. Hauback, "Counting electrons - a new approach to tailor the hydrogen sorption properties of high-entropy alloys," *Acta Mater.* **175**, 121–129 (2019).
- <sup>110</sup>H. Shen, J. Zhang, J. Hu, J. Zhang, Y. Mao, H. Xiao, X. Zhou, and X. Zu, "A novel TiZrHfMoNb high-entropy alloy for solar thermal energy storage," *Nanomaterials* **9**, 248 (2019).
- <sup>111</sup>C. Zhang, Y. Wu, L. You, X. Cao, Z. Lu, and X. Song, "Investigation on the activation mechanism of hydrogen absorption in TiZrNbTa high entropy alloy," *J. Alloys Compd.* **781**, 613–620 (2019).
- <sup>112</sup>P. Edalati, R. Floriano, A. Mohammadi, Y. Li, G. Zepon, H.-W. Li, and K. Edalati, "Reversible room temperature hydrogen storage in high-entropy alloy TiZrCrMnFeNi," *Scr. Mater.* **178**, 387–390 (2020).
- <sup>113</sup>J. Montero, G. Ek, L. Laversenne, V. Nassif, G. Zepon, M. Sahlberg, and C. Zlotea, "Hydrogen storage properties of the refractory Ti-V-Zr-Nb-Ta multi-principal element alloy," *J. Alloys Compd.* **835**, 155376 (2020).
- <sup>114</sup>C. Zhang, A. Song, Y. Yuan, Y. Wu, P. Zhang, Z. Lu, and X. Song, "Study on the hydrogen storage properties of a TiZrNbTa high entropy alloy," *Int. J. Hydrogen Energy* **45**, 5367–5374 (2020).
- <sup>115</sup>J. Hu, H. Shen, M. Jiang, H. Gong, H. Xiao, Z. Liu, G. Sun, and X. Zu, "A DFT study of hydrogen storage in high-entropy alloy TiZrHfScMo," *Nanomaterials* **9**, 461 (2019).
- <sup>116</sup>J. Hu, J. Zhang, H. Xiao, L. Xie, H. Shen, P. Li, J. Zhang, H. Gong, and X. Zu, "A density functional theory study of the hydrogen absorption in high entropy alloy TiZrHfMoNb," *Inorg. Chem.* **59**, 9774–9782 (2020).
- <sup>117</sup>A. Ferrari and F. Körmann, "Surface segregation in Cr-Mn-Fe-Co-Ni high entropy alloys," *Appl. Surf. Sci.* **533**, 147471 (2020).
- <sup>118</sup>M. F. Ashby and D. R. H. Jones, *Engineering Materials 1: An Introduction to Properties, Applications and Design* (Elsevier, 2012), Vol. 1.
- <sup>119</sup>B. J. K. N. Hammer and J. K. Nørskov, "Electronic factors determining the reactivity of metal surfaces," *Surf. Sci.* **343**, 211–220 (1995).
- <sup>120</sup>E. Osei-Agyemang and G. Balasubramanian, "Surface oxidation mechanism of a refractory high-entropy alloy," *NPJ Mater. Degrad.* **3**, 1–8 (2019).
- <sup>121</sup>P. Xie, Y. Yao, Z. Huang, Z. Liu, J. Zhang, T. Li, G. Wang, R. Shahbazian-Yassar, L. Hu, and C. Wang, "Highly efficient decomposition of ammonia using high-entropy alloy catalysts," *Nat. Commun.* **10**, 1–12 (2019).
- <sup>122</sup>Y. Yao, Z. Liu, P. Xie, Z. Huang, T. Li, D. Morris, Z. Finckro, J. Zhou, M. Jiao, J. Gao *et al.*, "Computationally aided, entropy-driven synthesis of highly efficient and durable multi-elemental alloy catalysts," *Sci. Adv.* **6**, 1–10 (2020).
- <sup>123</sup>P. Wynblatt and D. Chatain, "Modeling grain boundary and surface segregation in multicomponent high-entropy alloys," *Phys. Rev. Mater.* **3**, 054004 (2019).
- <sup>124</sup>T. A. Batchelor, J. K. Pedersen, S. H. Winther, I. E. Castelli, K. W. Jacobsen, and J. Rossmeisl, "High-entropy alloys as a discovery platform for electrocatalysis," *Joule* **3**, 834–845 (2019).
- <sup>125</sup>J. K. Pedersen, T. A. Batchelor, A. Bagger, and J. Rossmeisl, "High-entropy alloys as catalysts for the CO<sub>2</sub> and CO reduction reactions," *ACS Catal.* **10**, 2169–2176 (2020).
- <sup>126</sup>T. Löffler, A. Savan, A. Garzón-Manjón, M. Meischein, C. Scheu, A. Ludwig, and W. Schuhmann, "Toward a paradigm shift in electrocatalysis using complex solid solution nanoparticles," *ACS Energy Lett.* **4**, 1206–1214 (2019).
- <sup>127</sup>G. M. Tomboc, T. Kwon, J. Joo, and K. Lee, "High entropy alloy electrocatalysts: A critical assessment of fabrication and performance," *J. Mater. Chem. A* **8**, 14844–14862 (2020).